This is a preprint of: "Global dynamics of the Horava-Lifshitz cosmology in the presence of non-zero cosmological constant in a flat space", Fabao Gao, Jaume Llibre, *Phys. Dark. Universe*, vol. 38, 101139, 2022.
DOI: [10.1016/j.dark.2022.101139]

GLOBAL DYNAMICS OF THE HOŘAVA-LIFSHITZ COSMOLOGY IN THE PRESENCE OF NON-ZERO COSMOLOGICAL CONSTANT IN A FLAT SPACE

FABAO GAO[1,2], AND JAUME LLIBRE[2]

Abstract. Using the qualitative theory of differential equations, the global dynamics of a cosmological model based on Hořava-Lifshitz gravity is studied in the space with zero curvature in the presence of the non-zero cosmological constant. The study shows that there may be three unstable finite equilibrium positions under the Hořava-Lifshitz cosmology model and that the final evolution of the orbits of the cosmological model in the physical region of interest may tend towards some infinite equilibrium position, which may correspond to the late-time state of the universe.

1. Introduction

A decade ago Hořava [1] brought forward a new theory on space-time asymmetric gravitation, called Hořava-Lifshitz gravity, together with the scalar field theory of Lifshitz. This theory's applications to cosmology, dark energy, and black hole have stimulated many studies (See review papers [20], [21] or regular literature [2]-[19]).

Based on whether the value of Λ (cosmological constant) is zero and the flatness of the universe, i.e. whether the space curvature k is equal to zero, Leon et al. [8, 9, 10, 16] divided Hořava-Lifshitz cosmology into four cases: (1) $\Lambda = 0, k = 0$; (2) $\Lambda = 0, k \neq 0$; (3) $\Lambda \neq 0, k = 0$;

Key words and phrases. Global dynamics; Hořava-Lifshitz; non-zero cosmological constant.

(4) $\Lambda \neq 0, k \neq 0$ under the classic FLRW metric. They either studied partially the three-dimensional dynamics of Hořava-Lifshitz cosmology, or analyzed its two-dimensional dynamics under exponential potentials.

For the cosmological constant Λ that scientists have been concerning about, Carlip [22] argued that the vacuum fluctuations under the standard effective field theory produce a huge Λ and produce high k on the Planck scale, but it is almost invisible at the observable scale. Compared with the prediction in the standard Λ cold dark matter model, Valentino et al. [23] proposed that the cosmological space may be a closed three-dimensional sphere, i.e., the cosmological space's curvature may be positive, based on the enhanced lensing amplitude in the cosmic microwave background power spectra confirmed by Planck Legacy 2018 release [24]. Although this study provides the latest results, the debate about the universe's shape has not yet been settled. An important reason is that the calculation of the critical density of the universe depends on the measurement of the Hubble constant, which is different as estimated from different cosmological data. Then the boundary line of the universe is fuzzy. So it is too early to say that the universe must be closed.

The global dynamics of the Hořava-Lifshitz cosmology under the background of FLRW with $k = 0, \Lambda = 0$ was studied in [5], and the case of $k \neq 0, \Lambda = 0$ has also been addressed in [6]. In this paper we will consider the flat universe with $\Lambda \neq 0$. More precisely, in this paper we present the global dynamics of the Hořava-Lifshitz cosmology in the three-dimensional space including the infinity, neither partial or local dynamics, nor the two-dimensional case. The motivation for considering the cosmological constant and scalar field here is to fully explain the

universe's dynamic evolution and final state under the Hořava-Lifshitz gravitational model.

2. The cosmological equations

In order to describe the cosmological model, we first briefly review the Hořava-Lifshitz theory of gravity proposed in [1]. The field content in this theory can be derived from the space vector $\mathfrak{N}_i$ and scalar $\mathfrak{N}$, see [10, 11]. They are actually common 'lapse' and 'shift' variables in general relativity. From this the complete metric can be expressed as

$$ds^2 = -\mathfrak{N}^2 dt^2 + g_{ij}(dx^i + \mathfrak{N}^i dt)(dx^j + \mathfrak{N}^j dt), \quad \mathfrak{N}_i = g_{ij}\mathfrak{N}^j, \tag{1}$$

where g_{ij} is a spatial metric, here i and j are natural numbers from 1 to 3. The coordinate transformations follow $t \to l^3 t,\ x^i \to l x^i$. Note that g_{ij} is invariant, the same as $\mathfrak{N}$, but $\mathfrak{N}^i$ is scaled to $l^{-2}\mathfrak{N}_i$.

According to the detailed-balance condition, the full gravitational action of Hořava-Lifshitz is expressed as

$$\begin{aligned} S_g = & \int dt d^3x \sqrt{g}\mathfrak{N} \left\{ \frac{2}{\kappa^2}\left(K_{ij}K^{ij} - \lambda K^2\right) - \frac{\kappa^2}{2w^4} C_{ij}C^{ij} \right. \\ & + \frac{\mu\kappa^2}{2w^2}\frac{\epsilon^{ijk}}{\sqrt{g}} R_{il}\nabla_j R^l_k - \frac{\mu^2\kappa^2}{8} R_{ij}R^{ij} \\ & \left. - \frac{\mu^2\kappa^2}{8(3\lambda-1)}\left(\frac{1-4\lambda}{4}R^2 + \Lambda R - 3\Lambda^2\right)\right\}, \end{aligned} \tag{2}$$

where $C^{ij} = \epsilon^{ijk}\nabla_k\left(4R^j_i - R\delta^j_i\right)/(4\sqrt{g})$ denotes the Cotton tensor, $K_{ij} = (\dot{g}_{ij} - \nabla_i\mathfrak{N}_j - \nabla_j\mathfrak{N}_i)/(2\mathfrak{N})$ represents the extrinsic curvature, ϵ^{ijk} is the totally antisymmetric unit tensor, and $\epsilon^{ijk}/\sqrt{g}$ is the standard general covariant antisymmetric tensor, the indices can be raised or lowered using the metric g_{ij}. κ, λ, w and μ are all constants, for

more details see [1].

Consider the matter source action due to a scalar field, ϕ, as follows

$$S = \int dt d^3x \sqrt{g}\mathfrak{N}\left(\frac{3\lambda-1}{4}\frac{\dot{\phi}^2}{\mathfrak{N}^2} - V(\phi)\right), \tag{3}$$

and the metric $\mathfrak{N}^i = 0$, $g_{ij} = a^2(t)\gamma_{ij}$, $\gamma_{ij}dx^i dx^j = r^2 d\Omega_2^2 + dr^2/(1-kr^2)$. Here $a(t)$ represents the scale factor of the expanding universe, which is dimensionless, and γ_{ij} refers to the constant curvature metric with maximal symmetry. For the flat space we take $k = 0$ in this paper.

For the sake of simplicity, κ^2 and $\mathfrak{N}$ are normalized, and then the corresponding cosmological model can be interpreted as

$$\begin{aligned} H^2 &= \frac{\dot{\phi}^2}{24} + \frac{V(\phi)}{6(3\lambda-1)} - \frac{\mu^2\Lambda^2}{16(3\lambda-1)^2}, \\ \dot{H} + \frac{3}{2}H^2 &= -\frac{\dot{\phi}^2}{16} + \frac{V(\phi)}{4(3\lambda-1)} - \frac{3\mu^2\Lambda^2}{32(3\lambda-1)^2}, \\ \ddot{\phi} + 3H\dot{\phi} &+ \frac{2V'(\phi)}{3\lambda-1} = 0, \end{aligned} \tag{4}$$

where H is the Hubble parameter and has the form $\dot{a}(t)/a(t)$.

Considering that $V(\phi)$ admits various mathematical forms (see [9, 25, 26, 27]), we take $V(\phi) = (\varrho\phi)^{2n}/2n$ with a natural number n and a constant $\varrho > 0$ in this paper. Following [9, 10] we do the dimensionless transformation

$$\begin{aligned} x &= \frac{\dot{\phi}}{2\sqrt{6}H}, \quad y = \frac{\sqrt{V(\phi)}}{\sqrt{6}H\sqrt{3\lambda-1}}, \quad z = \frac{\Lambda\mu}{4(3\lambda-1)H}, \\ s &= -\frac{V'(\phi)}{V(\phi)}, \quad f(s) \equiv \frac{V''(\phi)}{V(\phi)} - \frac{V'(\phi)^2}{V(\phi)^2}. \end{aligned} \tag{5}$$

Thus we obtain $f(s) = -s^2/(2n)$, which is a power-law potential, so $ds/dN = \sqrt{6}xs^2/n$, here N denotes the new time variable. Furthermore it follows from equations (4) and (5) that

$$\begin{aligned} x^2 + y^2 - z^2 &= 1, \\ \frac{\dot{H}}{H} &= -3x^2. \end{aligned} \tag{6}$$

Therefore the field equations become the dimensionless form

$$\begin{aligned} \frac{dx}{dN} &= \sqrt{6}s\left(z^2 - x^2 + 1\right) + 3x\left(x^2 - 1\right), \\ \frac{dz}{dN} &= 3zx^2, \\ \frac{ds}{dN} &= \frac{\sqrt{6}}{n}xs^2. \end{aligned} \tag{7}$$

For more details on system (7) see the equations (205)-(207) of [9] or equations (52)-(54) of [16].

The present paper gives a fully description of the global dynamics of system (7) in the physical area of interest $G = \{(x, z, s) \in \mathbb{R}^3 : x^2 - z^2 \leq 1\}$. In sections 3 and 4 we will investigate the phase portraits of system (7) at finite and infinite equilibrium points on invariant planes and surface. In section 5 we will discuss the phase portraits of system (7) inside the Poincaré ball restricted to the region G. An introduction to the Poincaré ball that can be used to study the dynamics of the system (7) near infinity can be found in the appendix. Based on these sections, considering the symmetry of system (7), we will study the global dynamics of system (7) adding its behavior at infinity. Moreover we will give the final discussion and summary in the last section 6.

3. Phase portraits on two invariant planes $z = 0,\ s = 0$ and on the invariant surface $x^2 - z^2 = 1$

In order to understand the local phase portraits of equilibrium points (finite and infinite) and the global phase portraits of system (7) in the aforementioned region G (refer to [9] or [16] again), we begin to describe the phase portraits on the invariant planes $z = 0,\ s = 0$ and on the invariant surface $x^2 - z^2 = 1$.

From a dynamic point of view, if the initial point of universe evolution is on an invariant plane or an invariant surface, then the evolutionary trajectory of the universe will always remain on this plane or surface, which is why we call it "invariant".

3.1. **The invariant plane** $z = 0$**.** On the plane $z = 0$ system (7) reduces to

$$\begin{aligned} \frac{dx}{dN} &= (x^2 - 1)\left(3x - \sqrt{6}s\right), \\ \frac{ds}{dN} &= \frac{\sqrt{6}}{n} x s^2. \end{aligned} \tag{8}$$

The phase portrait of the above system in the strip $z = 0$ and $x^2 - z^2 \leq 1$ has been presented in [5] (see Figure 1). System (8) contains a hyperbolic equilibrium point $e_0 = (0, 0)$ and two semi-hyperbolic equilibrium points $e_1 = (1, 0)$, $e_2 = (-1, 0)$, where e_0 is a saddle point, and the other two are saddle-nodes.

3.2. **The invariant plane** $s = 0$**.** On the plane $s = 0$ system (7) reduces

$$\frac{dx}{dN} = 3x\left(x^2 - 1\right), \ \frac{dz}{dN} = 3zx^2. \tag{9}$$

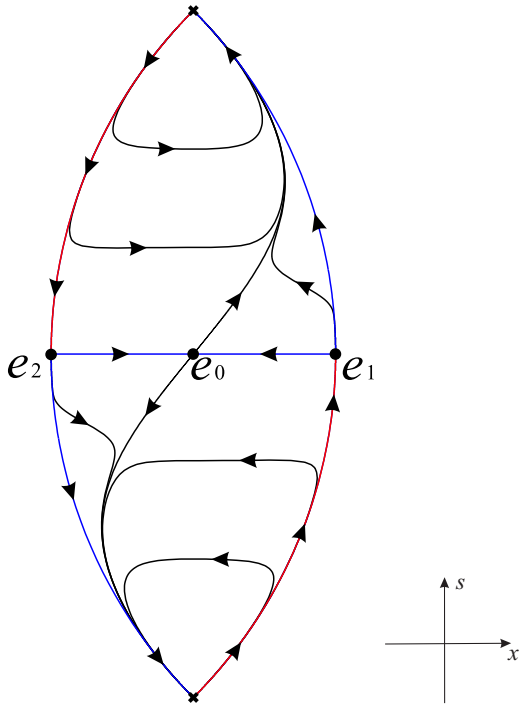

FIGURE 1. The phase portrait of system (7) on the invariant plane $z = 0$ in the region $-1 \leq x \leq 1$.

Note that each point on the line $x = 0$ is an equilibrium point. In order to eliminate the common factor x of the above equation. Introducing the transformation with respect to time $d\tau_1 = xdN$ yields

$$\frac{dx}{d\tau_1} = 3\left(x^2 - 1\right), \quad \frac{dz}{d\tau_1} = 3zx, \tag{10}$$

which has two hyperbolic equilibrium points $e_1 = (1, 0)$ and $e_2 = (-1, 0)$. Here e_1 is an unstable node and has two eigenvalues 3 and 6, but e_2 is a stable node and has eigenvalues -3 and -6.

According to the Poincaré compactification method (see Chapter 5 of [28] for more details), we perform the Poincaré transformation $x = 1/v$,

$z = u/v$ on the local chart U_1, then system (9) becomes

$$\frac{du}{dN} = 3uv^2, \ \frac{dv}{dN} = 3v\left(v^2 - 1\right). \tag{11}$$

The transformation can help us to plot the vector field of system (9) on the local chart U_1, and can also show the trajectory going to or coming from infinity. Since all the points at infinity (i.e. at $v = 0$) of system (11) are equilibrium points, we do the transformation of the time $d\tau_2 = vdN$, and the system (11) becomes

$$\frac{du}{d\tau_2} = 3uv, \ \frac{dv}{d\tau_2} = v^2 - 1. \tag{12}$$

However there is no equilibrium points in system (12).

System (9) on the local chart U_2 (Poincaré transformation $x = u/v$, $z = 1/v$) becomes

$$\frac{du}{dN} = -3uv^2, \ \frac{dv}{dN} = -3u^2v. \tag{13}$$

Since this system's linear term is always equal to zero, the corresponding topological index is known to be zero by the Poincaré-Hopf Theorem (for more details, see Theorem 6.30 in [28]). To study the local phase portrait of the equilibrium point (0,0) of system (13), we use the vertical blow-up techniques (see Ref. [29]), i.e., let $w = v/u$ then we have

$$\frac{du}{dN} = -3u^3w^2, \ \frac{dw}{dN} = 3u^2w(w^2 - 1). \tag{14}$$

Rescaling system (14)'s time variable N as $d\tau_3 = 3u^2wdN$, yields

$$\frac{du}{d\tau_3} = -uw, \ \frac{dw}{d\tau_3} = w^2 - 1. \tag{15}$$

This system admits two equilibrium points $(0,-1)$ and $(0,1)$ on $u=0$. Both of these two points are hyperbolic unstable saddle points with eigenvalues of $-2,\ 1$ and $2,\ -1$, respectively. The local phase portrait around them is shown in Figure 2(a). Note the time rescaling between the above two systems, the local phase portrait of system (14) can be found in Figure 2(b). Additionally, all points on the axes $u=0$ and $w=0$ are singularities of system (14). Since $u>0$ and $w>0$ in the first quadrant I of Figure 2(b), then $v=uw$ will decrease as u decreases, so the local phase portrait in the quadrant I of the u-w coordinate system (corresponding to system (14)) can be equivalently converted to the portrait in the first quadrant of the u-v coordinate system (corresponding to system (13)). Similarly the local phase portraits in the quadrants II, III and IV of the u-w coordinate system can also be equivalently converted to these portraits in the third, second and fourth quadrants of the u-v coordinate system, respectively. Therefore the local phase portrait of system (13) is displayed in Figure 2(c), and the corresponding local phase portrait at the origins of U_2 and the symmetrical V_2 in the invariant plane $s=0$ can be found in Figure 2(d).

In summary, considering that the straight lines $x=0$ and $z=0$ are invariant under the flow of system (9), we can obtain that in the Poincaré disk with $s=0$, the global phase portrait is restricted to the strip $-1\le x\le 1$ in Figure 3.

3.3. **The invariant surface $x^2-z^2=1$.** Under the flow of system (7), we first verify that $x^2-z^2=1$ is the invariant surface. If $\mathfrak{l}=\mathfrak{l}(x,z,s)=x^2-z^2-1$, then the surface $x^2-z^2=1$ is invariant, only

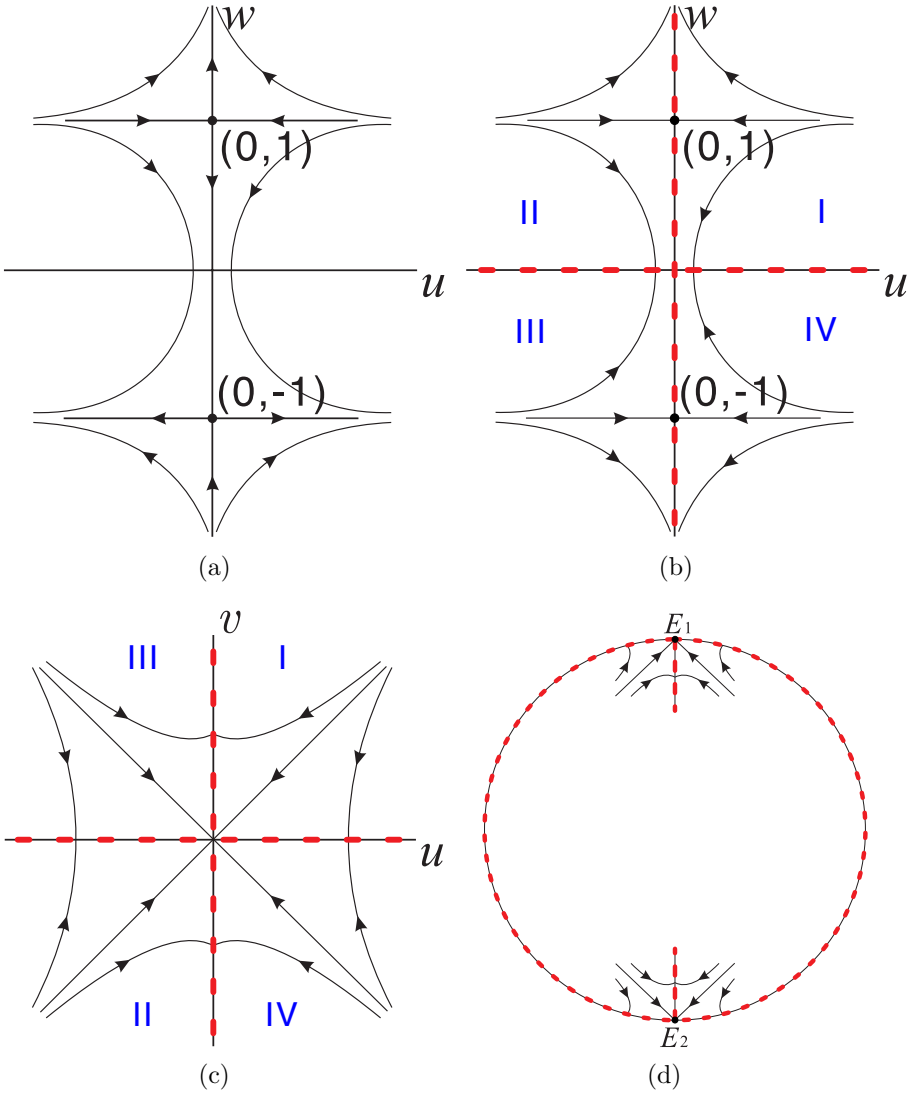

FIGURE 2. In (a), (b), and (c), there are the local phase portraits of the equilibrium points of systems (15), (14), and (13), respectively. In (d), there are the local phase portraits at the origins of U_2 and V_2 for $s = 0$.

if there exists a polynomial $\mathcal{P}$ satisfying the equation

$$\frac{\partial \mathfrak{l}}{\partial x}\frac{dx}{dN} + \frac{\partial \mathfrak{l}}{\partial z}\frac{dz}{dN} + \frac{\partial \mathfrak{l}}{\partial s}\frac{ds}{dN} = \mathcal{P}\mathfrak{l},$$

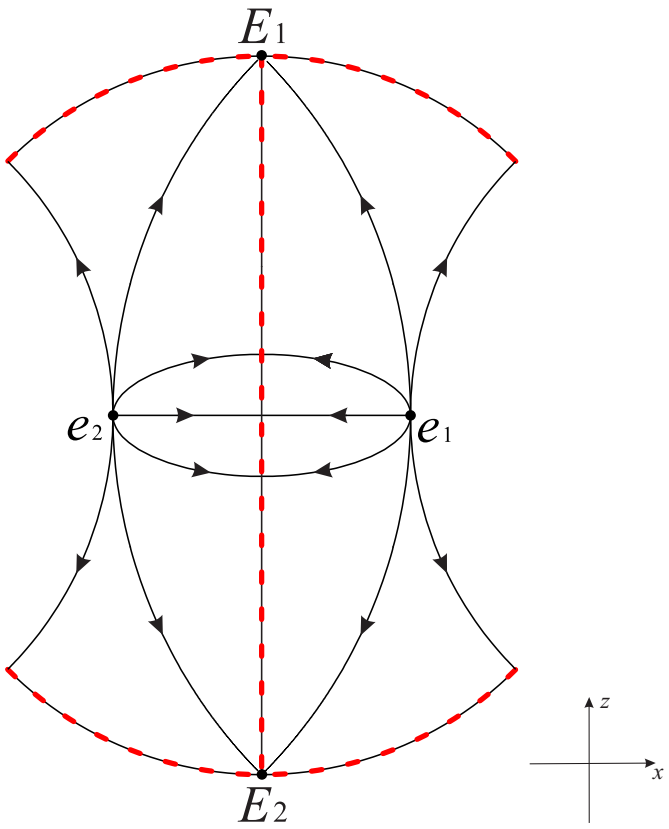

FIGURE 3. The phase portrait restricted to the region $x^2 - z^2 \leq 1$ on the invariant plane $s = 0$ inside the Poincaré disc.

which is exactly the case with $\mathcal{P} = 2x(3x - \sqrt{6}s)$. The polynomial here is derived with the help of the software Mathematica, and more information on invariance can be found in [28].

On the surface $x^2 - z^2 = 1$ system (7) writes

$$\frac{dx}{dN} = 3x\left(x^2 - 1\right), \quad \frac{ds}{dN} = \frac{\sqrt{6}}{n}\, xs^2. \tag{16}$$

Then except for s-axis that is filled with equilibrium points, the above system also has two finite semi-hyperbolic equilibrium points $e_1 = (1, 0)$

and $e_2 = (-1, 0)$. It follows from Theorem 2.19 of [28] that both e_1 and e_2 are saddle-nodes.

System (16) on the local chart U_1 can be written as

$$\frac{du}{dN} = u\left[\frac{\sqrt{6}}{n}u + 3\left(v^2 - 1\right)\right], \ \frac{dv}{dN} = 3v\left(v^2 - 1\right). \tag{17}$$

This system admits two infinite hyperbolic equilibrium points $e_5 = (0, 0)$ and $e_6 = (\sqrt{6}n/2, 0)$, where e_5 is a stable node and has eigenvalues -3 of multiplicity two, and the other point e_6 is an unstable saddle and has two eigenvalues ± 3.

System (16) on the local chart U_2 can be written as

$$\frac{du}{dN} = u\left[-\frac{\sqrt{6}}{n}u + 3\left(u^2 - v^2\right)\right], \ \frac{dv}{dN} = -\frac{\sqrt{6}}{n}uv. \tag{18}$$

Rescaling the time $d\tau_4 = udN$ we have

$$\frac{du}{d\tau_4} = -\frac{\sqrt{6}}{n}u + 3\left(u^2 - v^2\right), \ \frac{dv}{d\tau_4} = -\frac{\sqrt{6}}{n}v. \tag{19}$$

The origin $(0, 0)$ of the above system is a hyperbolic stable node with eigenvalues $-\sqrt{6}/n$ and a multiplicity of 2. In this way, the origin $e_7 = (0, 0)$ of system (18) has a local phase portrait as shown in Figure 4.

In summary the global phase portraits of system (16) is integrated in Figure 5.

3.4. **The finite equilibrium points.** System (7) allows three three-dimensional finite equilibrium points $p_0 = (0, 0, 0)$, $p_1 = (1, 0, 0)$ and $p_2 = (-1, 0, 0)$, p_0 has eigenvalues $-3, 0, 0$, p_1 and p_2 have the same eigenvalues $6, 3, 0$. Here p_1 and p_2 are the intersection points of $x^2 - z^2 = 1$, $s = 0$ and $z = 0$ that were just studied in the previous subsections

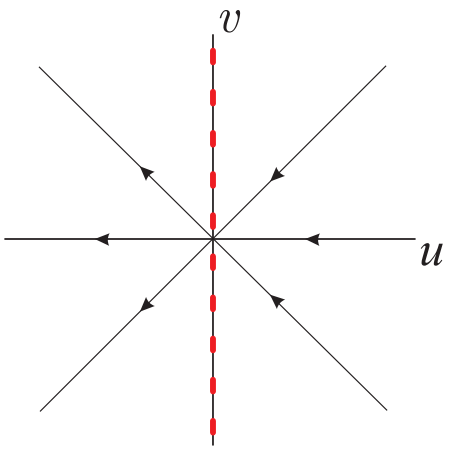

FIGURE 4. The local phase portrait at the origin of U_2 for $x^2 - z^2 = 1$.

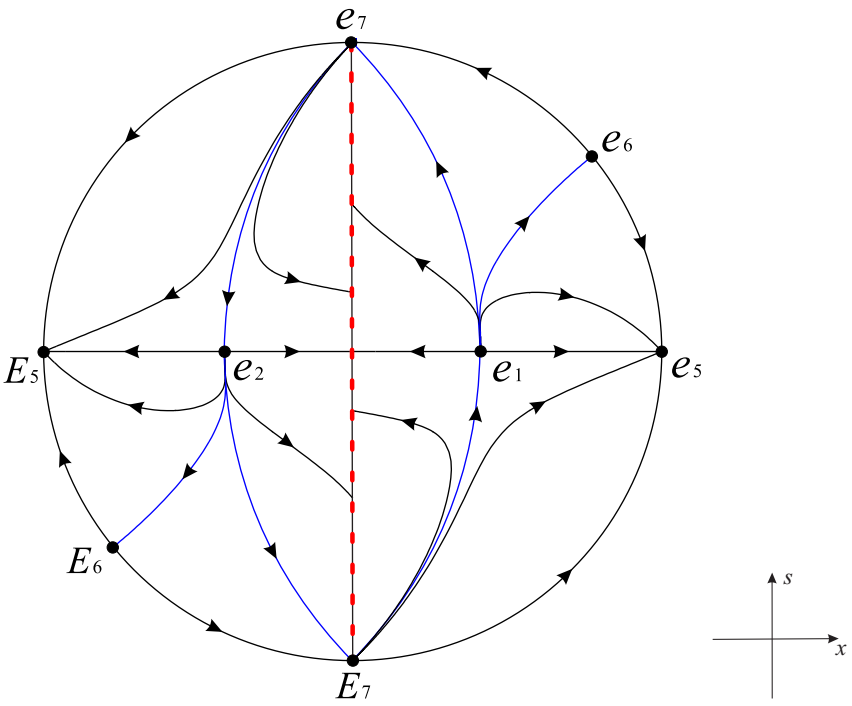

FIGURE 5. Phase portrait on the invariant surface $x^2 - z^2 = 1$.

3.1-3.3, that is, p_1 and p_2 are the equilibrium points e_1 and e_2, respectively. The origin p_0 is located in the middle of the intersection of $z = 0$ and $s = 0$, and it is the equilibrium point e_0 studied in the previous subsection 3.1.

4. Phase portrait on the surface of Poincaré ball at infinity

The three-dimensional Poincaré compactification (see Appendix or [30] for more details) is used to study the dynamics of the system (7) near infinity in this section. So we have $x = 1/z_3,\ z = z_1/z_3,\ s = z_2/z_3$ on the local chart U_1, and then system (7) on the U_1 is reduced to

$$\begin{aligned} \frac{dz_1}{dN} &= z_1\left[3z_3^2 - \sqrt{6}z_2\left(-1 + z_1^2 + z_3^2\right)\right], \\ \frac{dz_2}{dN} &= z_2\left[3\left(z_3^2 - 1\right) + \sqrt{6}z_2\left(\frac{1+n}{n} - z_1^2 - z_3^2\right)\right], \\ \frac{dz_3}{dN} &= z_3\left[3\left(z_3^2 - 1\right) + \sqrt{6}z_2\left(1 - z_1^2 - z_3^2\right)\right]. \end{aligned} \tag{20}$$

In different local charts, $z_3 = 0$ corresponds to the infinity of $\mathbb{R}^3$. The equilibrium points of the system (20) are listed in Table 1, where the equilibrium point u_{31} represents the origin of the local chart U_3, and the other equilibrium points lie in the local chart U_1. Additionally, for any constant a, u_{a0} means that $s = 0$ on local chart U_1 is filled with equilibrium points.

For the case $z_3 = 0$ system (20) becomes

$$\begin{aligned} \frac{dz_1}{dN} &= \sqrt{6}z_1z_2\left(1 - z_1^2\right), \\ \frac{dz_2}{dN} &= z_2\left[-3 + \sqrt{6}z_2\left(\frac{1+n}{n} - z_1^2\right)\right]. \end{aligned} \tag{21}$$

TABLE 1. The equilibrium points on the local charts of the surface of the Poincaré ball at $\mathbb{R}^3$ infinity.

Equilibrium points	**Eigenvalues**
$u_{11} = (0, 0, 0)$	$-3, -3, 0$
$u_{12} = \left(-1, \frac{\sqrt{6}}{2}n, 0\right)$	$-3, 3, -6n$
$u_{13} = \left(1, \frac{\sqrt{6}}{2}n, 0\right)$	$-3, 3, -6n$
$u_{14} = \left(0, \frac{\sqrt{6}n}{2(n+1)}, 0\right)$	$-\frac{3}{n+1}, \frac{3n}{n+1}, 3$
$u_{a0} = (a, 0, 0)$	$-3, -3, 0$
$u_{31} = (0, 0, 0)$	$0, 0, 0$

Rescaling the time $d\tau_5 = z_2 dN$, system (20) is reduced to

$$\begin{aligned} \frac{dz_1}{d\tau_5} &= \sqrt{6} z_1 \left(1 - z_1^2\right), \\ \frac{dz_2}{d\tau_5} &= -3 + \sqrt{6} z_2 \left(\frac{1+n}{n} - z_1^2\right). \end{aligned} \tag{22}$$

Then system (22) allows equilibrium points $e_{i,1}$, $e_{i,2}$ and $e_{i,3}$, the coordinates of which are $(\mp 1, \sqrt{6}n/2)$ and $(0, \sqrt{6}n/(2n+2))$, respectively. Note that the subscript "i" here has no special meaning. Although the corresponding equilibrium points are indeed on the infinite Poincaré sphere, they are just to distinguish them from the equilibrium points on the invariant planes and surface. The equilibrium points $e_{i,1}$ and $e_{i,2}$ are hyperbolic unstable saddles with eigenvalues 3 and $-6n$, and the equilibrium point $e_{i,3}$ is a hyperbolic unstable node with eigenvalues $3n/(1+n)$ and 3. The phase portrait on local chart U_1 of the Poincaré sphere at infinity is shown in Figure 6.

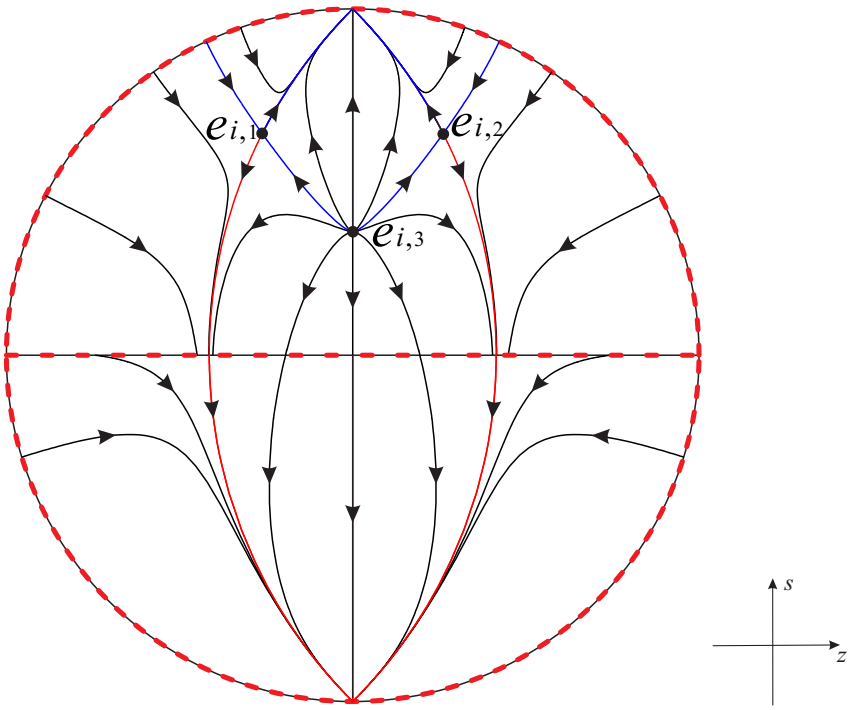

FIGURE 6. The phase portrait of system (7) on the local chart U_1 at infinity.

On the local chart U_2 we have Poincaré compactification $x = z_1/z_3,\ z = 1/z_3,\ s = z_2/z_3$, the system (7) becomes

$$
\begin{aligned}
\frac{dz_1}{dN} &= -z_1 z_3^2 + \sqrt{6} z_2 \left(1 - z_1^2 + z_3^2\right), \\
\frac{dz_2}{dN} &= z_1 z_2 \left(-3 z_1 + \frac{\sqrt{6}}{n} z_2\right), \\
\frac{dz_3}{dN} &= -3 z_1^2 z_3.
\end{aligned} \tag{23}
$$

To study the phase portrait at infinity we take $z_3 = 0$, and changing the time $d\tau_6 = z_2 dN$ system (23) is equivalent to

$$\begin{aligned} \frac{dz_1}{d\tau_6} &= \sqrt{6}\,(1 - z_1^2)\,, \\ \frac{dz_2}{d\tau_6} &= z_1 \left(-3z_1 + \frac{\sqrt{6}}{n} z_2 \right). \end{aligned} \tag{24}$$

Since $(0, 0)$ is the non-equilibrium point of system (24), there is no need to continue to investigate the equilibrium points at infinity in U_2. These have been discussed in the chart U_1.

On the local chart U_3 we have Poincaré compactification $x = z_1/z_3,\ z = z_2/z_3,\ s = 1/z_3$, then system (7) writes

$$\begin{aligned} \frac{dz_1}{dN} &= z_1 \left[-\frac{\sqrt{6}(1+n)}{n} z_1 + 3z_1^2 - 3z_3^2 \right] + \sqrt{6}\,(z_2^2 + z_3^2)\,, \\ \frac{dz_2}{dN} &= z_1 z_2 \left(-\frac{\sqrt{6}}{n} + 3z_1 \right), \\ \frac{dz_3}{dN} &= -\frac{\sqrt{6}}{n} z_1 z_3. \end{aligned} \tag{25}$$

It can be followed from system (25) that

$$\begin{aligned} \frac{dz_1}{dN} &= z_1 \left[-\frac{\sqrt{6}(1+n)}{n} z_1 + 3z_1^2 \right] + \sqrt{6} z_2^2, \\ \frac{dz_2}{dN} &= z_1 z_2 \left(-\frac{\sqrt{6}}{n} + 3z_1 \right). \end{aligned} \tag{26}$$

Note that the origin $(0, 0)$ is a linearly zero equilibrium point of the above system. According to the Poincaré-Hopf Theorem, the topological index is zero. The vertical blow-up technique will be applied to

investigate its local phase portrait. Then defining $w = z_2/z_1$ we have

$$\begin{aligned} \frac{dz_1}{dN} &= z_1^2\left[\sqrt{6}\left(-\frac{1+n}{n}+w^2\right)+3z_1\right], \\ \frac{dw}{dN} &= \sqrt{6}z_1 w\left(w^2-1\right). \end{aligned} \tag{27}$$

Rescaling the time $d\tau_7 = z_1 dN$ and eliminating the common factor z_1 of system (27), then we obtain

$$\begin{aligned} \frac{dz_1}{d\tau_7} &= z_1\left[\sqrt{6}\left(-\frac{1+n}{n}+w^2\right)+3z_1\right], \\ \frac{dw}{d\tau_7} &= \sqrt{6}w\left(w^2-1\right). \end{aligned} \tag{28}$$

Since there are three hyperbolic equilibrium points $e_{i,4} = (0,-1)$, $e_{i,5} = (0,1)$ and $e_{i,6} = (0,0)$ of system (28) on $z_1 = 0$, the previous two are stable nodes with eigenvalues of $-2\sqrt{6}$ and $-\sqrt{6}/n$, the last one is an unstable saddle point with eigenvalues of $-\sqrt{6}(n+1)/n$ and $\sqrt{6}$. We note that this is the same as the equilibrium points in the system (26) of reference [6]. So the local phase portraits of systems (28), (27) and (26) are shown in Figures 7(a), 7(b) and 7(c), respectively, and Figure 8 shows the phase portrait at the origin of the local chart U_3.

Combined with the previous discussion, Figure 9 shows the global phase portrait at infinity on the Poincaré sphere.

5. Phase portraits within the Poincaré sphere conditioned to $x^2 - z^2 \leq 1$

The dynamical system (7) is invariant under the two symmetry transfromations about the origin and the z-axis, i.e., $(x,z,s) \mapsto (-x,-z,-s)$ and $(x,z,s) \mapsto (-x,z,-s)$. So we divide the Poincaré ball restricted

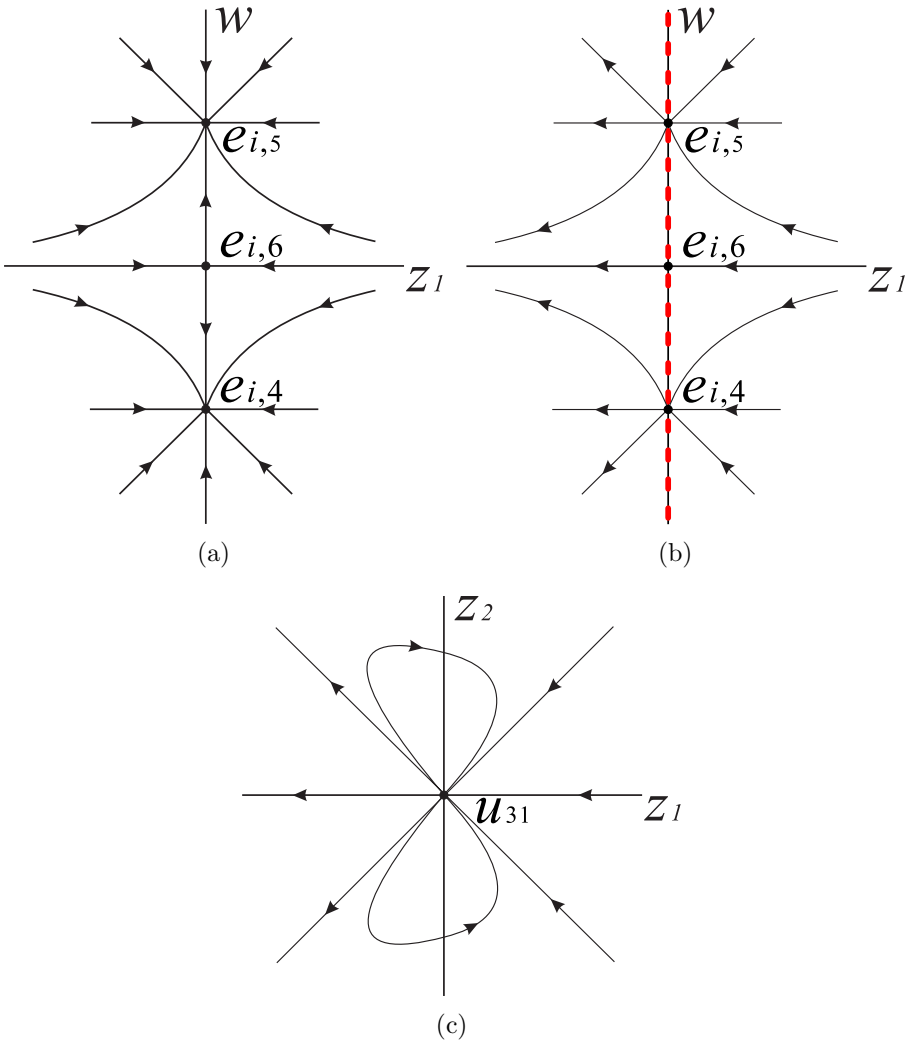

FIGURE 7. The local phase portraits (a), (b), and (c) of the above equilibrium points correspond to systems (28), (27), and (26), respectively.

to the region G into four regions as follows

$$R_1: \ z \le 0, \ s \ge 0. \quad R_3: \ z \ge 0, \ s \ge 0.$$
$$R_2: \ z \le 0, \ s \le 0. \quad R_4: \ z \ge 0, \ s \le 0.$$

In view of the aforementioned symmetries, we only need to focus on the phase portrait of system (7) in one region (such as R_1).

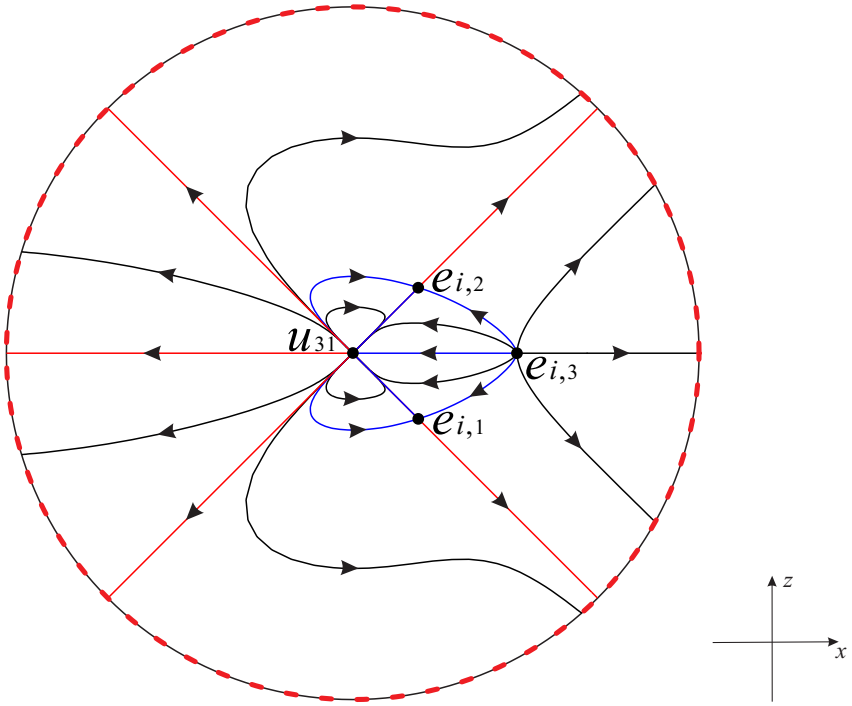

FIGURE 8. The phase portrait of system (7) in the local chart U_3 at infinity.

Combining the phase portrait in the invariant planes $s = 0$, and $z = 0$ with the phase portrait in the invariant surface $x^2 - z^2 = 1$, and the phase portrait at infinity, the phase portrait on the boundary surface of R_1 is as shown in Figure 10. Now we divide the boundary surface of the region R_1 into six parts (see Figure 11 for more details), to show the phase portrait of R_1 more clearly. It can be found from Figures 10(a) and 10(b) that the equilibrium point u_{31} of the Poincaré ball is stable on the front boundary surfaces F_1 and F_2, and there is a stable parabolic sector and an elliptic sector segment F_3. However, on the back boundary surfaces B_1 and B_2, the north pole u_{31} is unstable.

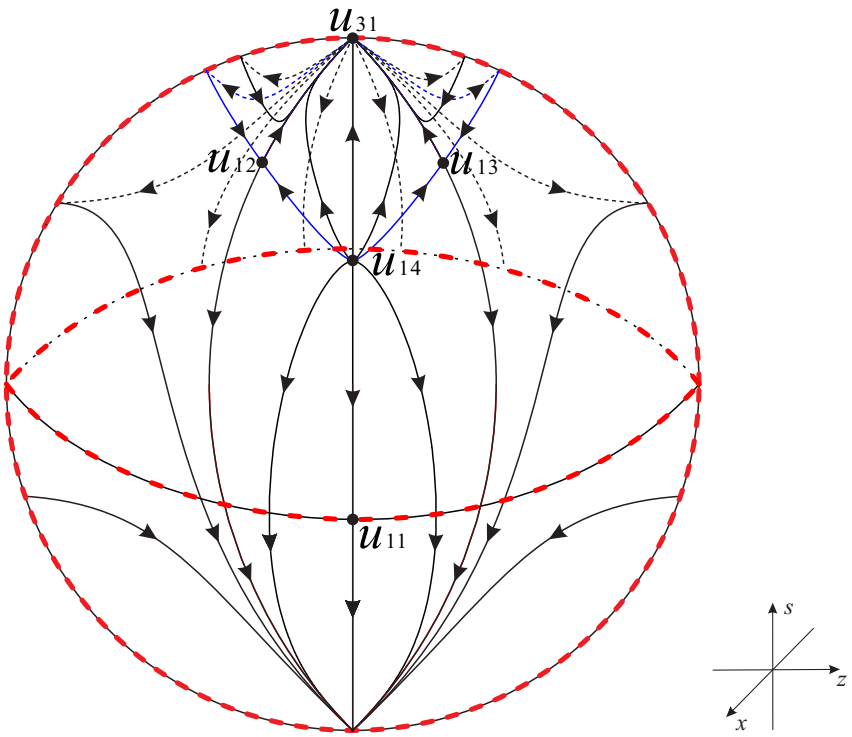

FIGURE 9. The global phase portrait of system (7) on the Poincaré sphere at infinity.

5.1. **Dynamics inside the region R_1.** System (7) has three finite equilibrium points p_0, p_1 and p_2. The dynamical behavior of system (7) in the Interior of the region R_1 depends on the comprehensive performance of the flow in the surface and planes

$$h(x,z,s)=0,\ x=0,\ z=0,\ s=0,$$

where

$$h(x,z,s) \ = \sqrt{6}s\left(z^2-x^2+1\right)+3x\left(x^2-1\right).$$

The above planes and surface cut the region R_1 into four different subregions $S_i,\ i=(1,\ldots,4)$, see Figures 12 and 13 for more details. It is noted that $h<0$ in the subregions S_1 and S_4, and $h>0$ in the

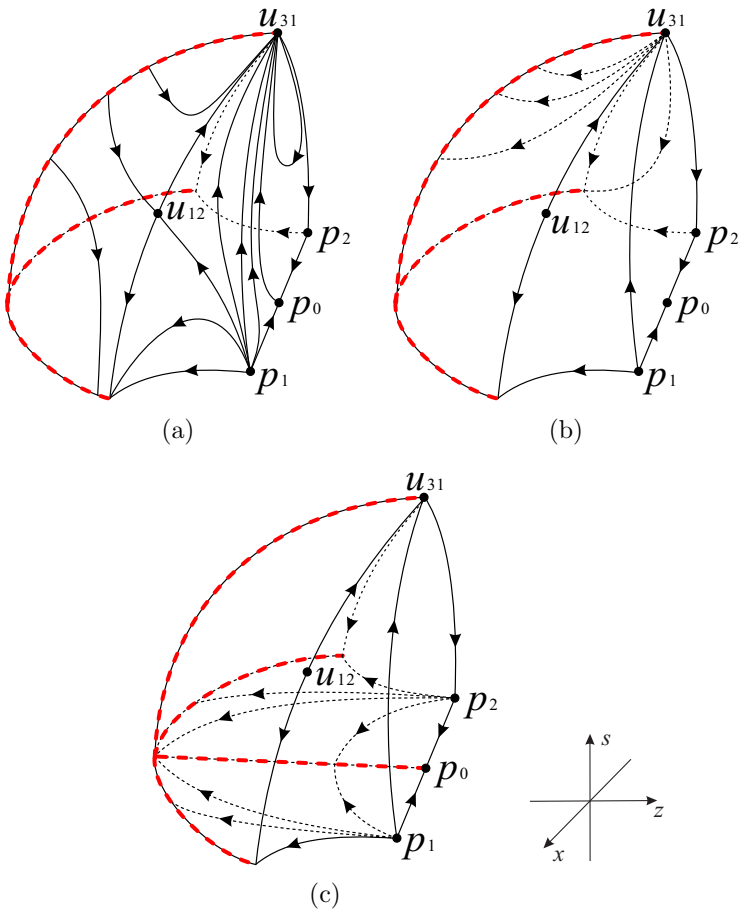

FIGURE 10. Phase portraits on the boundary surface R_1: (a). The front boundary surface; (b). The back boundary surface; (c). The bottom plane.

subregions S_2 and S_3. To avoid confusion, please note that the solid and dotted lines in Figure 13 is consistent with those in Figure 12.

As it is shown in S_1 (see Figure 13(a)) the upper surface is included in the blue surface $h = 0$, and the bottom plane is included in the invariant plane $s = 0$. According to Table 2, the orbits monotonically decrease in the x and z directions. In the s direction, they monotonically increase, so the orbits in the subregion S_1 can only start at the finite equilibrium point p_1 and pass through the upper surface of S_1 into the subregion

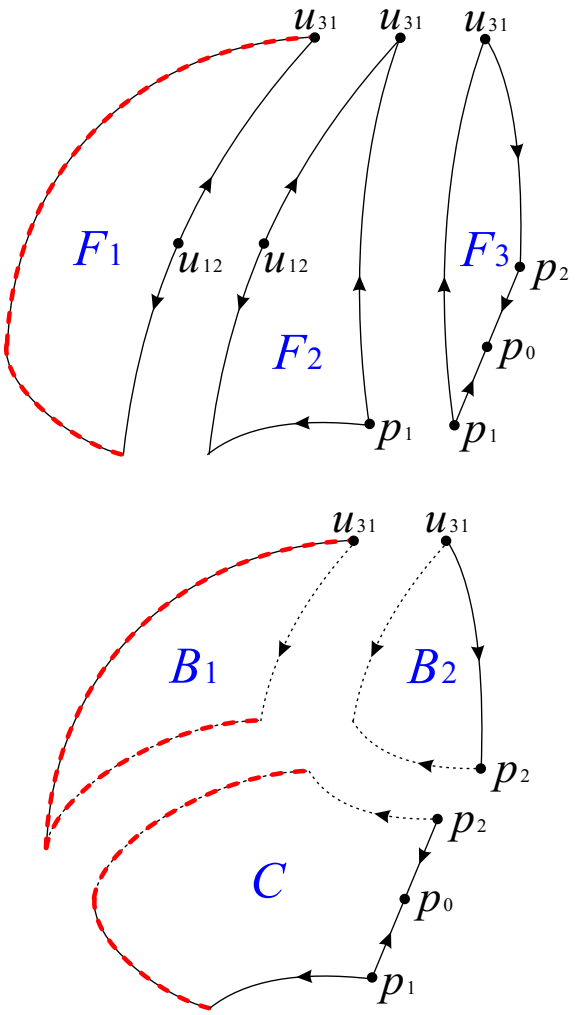

FIGURE 11. The six boundaries of R_1.

S_2. However in subregion S_2 (see Figure 13(b), i.e. the remaining part after S_1 is extracted from the region R_1 when $x > 0$, the orbits monotonically increase in the x and s directions but monotonically decrease in the z-direction. So we find that the orbits in S_2 can only start at p_1 or the equilibrium points on the negative z-axis, and they eventually move towards the infinity equilibrium point u_{12} fixed on the surface of S_2. Therefore the dynamic behavior of the orbits on these

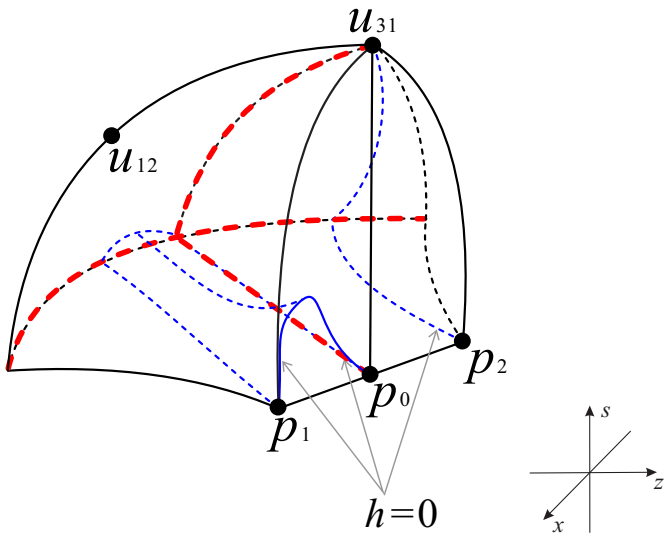

FIGURE 12. There are four subregions inside the region R_1 of the Poincaré ball.

two subregions can be represented in the following form

$$\begin{array}{ccccccc} & & p_1 & & & & \\ & \swarrow & & \searrow & & & \\ S_1 & \longrightarrow & & S_2 & \longrightarrow & u_{12} & \longleftarrow \text{ negative } z\text{-axis.} \end{array}$$

TABLE 2. The dynamics of the four subregions.

Subregions	**Associated Region**	**Monotonicity**
S_1	$h<0,\ x>0,\ z<0,\ s>0$	$\dot{x}<0,\ \dot{z}<0,\ \dot{s}>0$
S_2	$h>0,\ x>0,\ z<0,\ s>0$	$\dot{x}>0,\ \dot{z}<0,\ \dot{s}>0$
S_3	$h>0,\ x<0,\ z<0,\ s>0$	$\dot{x}>0,\ \dot{z}<0,\ \dot{s}<0$
S_4	$h<0,\ x<0,\ z<0,\ s>0$	$\dot{x}<0,\ \dot{z}<0,\ \dot{s}<0$

In subregion S_3 (see Figure 13(c)) the left vertical plane facing us is contained in the plane $x=0$, and the right vertical plane is contained

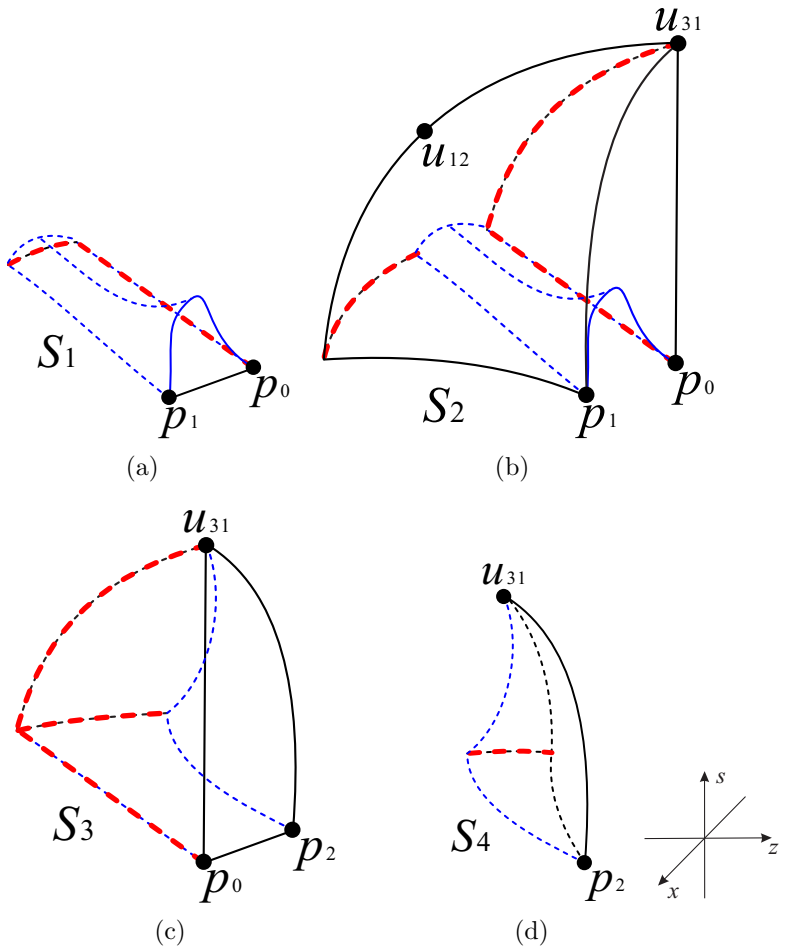

FIGURE 13. The four subregions S_i of R_1 $(i = 1 \cdots, 4)$.

in the invariant plane $z = 0$. In the opposite surfaces the left one is included in the surface of the Poincaré sphere, and the right one is included in the surface $h = 0$. Since the orbits in S_3 monotonically decrease in the z and s directions, and they increase monotonically in the x direction, it follows that the orbits will eventually go to the equilibrium point which lie in the equator or go to the negative z-axis in that region, and the orbits in this region may only come from the adjacent subregion S_4 (see Figure 13(d)). The left and right surfaces

of subregion S_4 belong to the surfaces $h = 0$ and $x^2 - z^2 = 1$ $(x < 0)$, respectively. Since all the orbits are monotonically decreasing in S_4, the orbits in this region arrive from the infinite equilibrium point u_{31}, i.e. north pole of the Poincaré ball, and tend to the infinite equilibrium points on the equator of this region at a future date, or enter into the subregion S_3. This dynamical behavior can be represented as follows

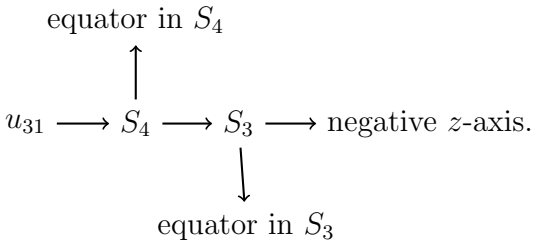

Therefore the orbits' dynamic behavior inside the four subregions of R_1 investigated above can be condensed to

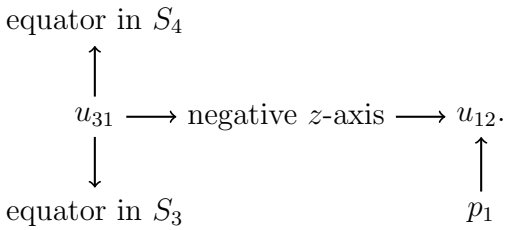

This flow chart states clearly that the orbits of system (7) included in R_1 have α-limit at p_1 and the north pole u_{31} (also referred to as past attractors or negative attractors) of the Poincaré sphere. Additionally the orbits have ω-limit either at u_{12} (also called future attractor or positive attractor), or other infinite equilibrium points on the equator of subregions S_3 and S_4, which are located at the intersection of the Poincaré ball and at the infinity of the invariant planes $s = 0$ in $\mathbb{R}^3$ when $x < 0$, see Figure 12 or Figures 13(c) and 13(d).

Therefore all the global dynamical behavior of the system (7) is represented qualitatively and completely.

6. Conclusions

In the present paper we have fully described the global phase portrait of Hořava-Lifshitz cosmology in the presence of non-zero cosmological constant and zero curvature in the region of physical interest G. By taking the fact that the cosmological equations remains invariant under the two symmetries mentioned in section 5, the global phase portrait of the cosmological model in G is provided completely.

From the perspective of cosmology, combining the phase portrait analysis of system (7) in Sections 3-5 and the formulations of the density parameter and the equation-of-state parameter of dark energy in [10], we know that the unstable finite equilibrium points p_1 and p_2 are dominated by dark matter with negligible dark energy, and the finite equilibrium p_0 located on the equilibrium point line may also be characterized by more physical dark matter if the initial conditions are not in the invariant plane $z = 0$. Besides the initial conditions in the invariant planes $s = 0$ and $z = 0$ as well as on the backside of the invariant surface $x^2 - z^2 = 1$, the phase portrait displays that the eventual evolution of the orbits of the cosmological model in G tends to the infinite equilibrium point u_{12}, which can be the late-time state of the universe and to other infinite equilibrium points placed at the equator of the Poincaré ball. For the Hořava-Lifshitz gravity in a FLRW space-time with $k = 0$ and $\Lambda \neq 0$, equations (5) implies that the Hubble parameter H tends to zero in forward time in this cosmological model, and this is an important difference between the Hořava-Lifshitz model

and the standard ΛCDM model where the universe evolves to a purely Λ-dominated state with constant non-zero Hubble parameter.

Appendix: The Poincaré compactification in $\mathbb{R}^3$ [28]

For a polynomial vector field $X= (P_1, P_2, P_3)$, and the degree $n = \max\{\deg(P_i) : i = 1, 2, 3\}$, its differential system is

$$\frac{dx}{dN} = P_1(x, y, z),\ \frac{dy}{dN} = P_2(x, y, z),\ \frac{dz}{dN} = P_3(x, y, z).$$

Defining the unit sphere in $\mathbb{R}^4$ by $\mathbb{S}^3 = \{y = (y_1, y_2, y_3, y_4) \in \mathbb{R}^4 : \|y\| = 1\}$, we denote the northern hemisphere by $\mathbb{S}_+ = \{y \in \mathbb{S}^3 : y_4 > 0\}$, the southern hemisphere by $\mathbb{S}_- = \{y \in \mathbb{S}^3 : y_4 < 0\}$, the equator of $\mathbb{S}^3$ by the 2-sphere $\mathbb{S}^2 = \{y \in \mathbb{S}^3 : y_4 = 0\}$, the tangent space at the point y of $\mathbb{S}^3$ by $T_y\mathbb{S}^3$. Hence the tangent hyperplane $T_{(0,0,0,1)}\mathbb{S}^3 = \{(x_1, x_2, x_3, 1) \in \mathbb{R}^4 : (x_1, x_2, x_3) \in \mathbb{R}^3\}$ is identified with $\mathbb{R}^3$. Moreover let

$$f_+ : \mathbb{R}^3 = T_{(0,0,0,1)}\mathbb{S}^3 \to \mathbb{S}+, \quad f_+(x) = \frac{1}{\Delta x}(x_1, x_2, x_3, 1),$$

and

$$f_- : \mathbb{R}^3 = T_{(0,0,0,1)}\mathbb{S}^3 \to \mathbb{S}-, \quad f_-(x) = -\frac{1}{\Delta x}(x_1, x_2, x_3, 1),$$

be the two central projections, where $\Delta x = \left(\sum_{i=1}^3 x_i^2 + 1\right)^{1/2}$. Then f_+ and f_- are identified by $\mathbb{R}^3$ with the two hemispheres of $\mathbb{S}^3$. These two central projections clarify two transcripts of X, i.e. $Df_+ \circ X$ in $\mathbb{S}_+$, and $Df_- \circ X$ in $\mathbb{S}_-$. Let $\widetilde{X}$ be the vector field on $\mathbb{S}^3 \backslash \mathbb{S}^2 = \mathbb{S}_+ \cup \mathbb{S}_-$.

Now we analytically continue the vector field $\widetilde{X}(y)$ to the entire sphere $\mathbb{S}^3$ by $p(X)(y) = y_4^{n-1}\widetilde{X}(y)$. The continued vector field $p(X)$ is named *Poincaré compactification* of X. We note that the infinity

of $\mathbb{R}^3$ represented by $\mathbb{S}^2$ is invariant for the vector field $p(X)$. The compactification for polynomial vector fields in $\mathbb{R}^2$ was introduced by Poincaré, and one can find its extension to $\mathbb{R}^m$ from [30]. Next we shall study the orthogonal projection of the closed $\mathbb{S}_+$ to $y_4 = 0$, which is a closed ball B (designated Poincaré ball) with radius 1, its inner area is diffeomorphic to $\mathbb{R}^3$, and its boundary surface $\mathbb{S}^2$ is identified with $\mathbb{R}^3$ at infinity.

Since $\mathbb{S}^3$ is a differentiable manifold, we must consider eight local charts (U_i, F_i) and (V_i, G_i) in order to study the dynamics of $p(X)$, where

$$U_i = \{y \in \mathbb{S}^3 : y_i > 0\}, \quad V_i = \{y \in \mathbb{S}^3 : y_i < 0\},$$

and the diffeomorphisms

$$F_i : U_i \to \mathbb{R}^3, \quad G_i : V_i \to \mathbb{R}^3 \quad \text{for } i = 1, 2, 3, 4,$$

are the central projections' inverses from the origin to the center of the tangent planes at the points $(\pm 1, 0, 0, 0)$, $(0, \pm 1, 0, 0)$, $(0, 0, \pm 1, 0)$ and $(0, 0, 0, \pm 1)$, respectively. Then the expression of $p(X)$ in the local chart U_1 is

$$\frac{z_3^n}{(\Delta z)^{n-1}}(-z_1 P_1 + P_2, -z_2 P_1 + P_3, -z_3 P_1),$$

where $P_i = P_i(1/z_3, z_1/z_3, z_2/z_3)$. In the local chart U_2 we have

$$\frac{z_3^n}{(\Delta z)^{n-1}}(-z_1 P_2 + P_1, -z_2 P_2 + P_3, -z_3 P_2),$$

where $P_i = P_i(z_1/z_3, 1/z_3, z_2/z_3)$. In the local chart U_3 we obtain

$$\frac{z_3^n}{(\Delta z)^{n-1}}(-z_1 P_3 + P_1, -z_2 P_3 + P_2, -z_3 P_3),$$

where $P_i = P_i(z_1/z_3, z_2/z_3, 1/z_3)$. In the local chart U_4 we get

$$z_3^{n-1}(P_1, P_2, P_3),$$

where $P_i = P_i(z_1, z_2, z_3)$. Furthermore the demonstration of $p(X)$ in the local chart V_i is the same as in the U_i multiplied by $(-1)^{n-1}$.

In addition the above factor $1/(\Delta z)^{n-1}$ is omitted by doing a time rescaling when we use the expressions of the compactified vector field $p(X)$ in the local charts.

Acknowledgments

The first author was supported by the National Natural Science Foundation of China (NSFC) through grants 12172322 and 11672259, the China Scholarship Council through grant 201908320086.

The second author was supported by the Ministerio de Economía, Industria y Competitividad, Agencia Estatal de Investigación grants MTM2016-77278-P (FEDER) and MDM-2014-0445, the Agència de Gestió d'Ajuts Universitaris i de Recerca grant 2017SGR1617, and the H2020 European Research Council grant MSCA-RISE-2017-777911.

The authors are very grateful to the extremely careful anonymous reviewers whose comments and suggestions helped improve and clarify this paper.

Conflicts of Interest: The authors declare no conflict of interest.

References

[1] P. Hořava, Quantum gravity at a Lifshitz point, *Physical Review D* **79**, 084008, 2009.

[2] E.M.C. Abreu, A.C.R. Mendes, G. Oliveira-Neto et al., Hořava-Lifshitz cosmological models with noncommutative phase space variables, *General Relativity and Gravitation* **51**, 95, 2019.

[3] S. Carloni, E. Elizalde and P.J. Silva, An analysis of the phase space of Hořava-Lifshitz cosmologies. In: S.D. Odintsov, D. Sáez-Gómez and S. Xambó-Descamps (eds) Cosmology, Quantum Vacuum and Zeta Functions, *Springer Proceedings in Physics* **137**, 139-148, Springer-Verlag, Berlin, 2011.

[4] B. Chen, On Hořava-Lifshitz cosmology, *Chinese Physics C* **35**(5), 429-435, 2011.

[5] F.B. Gao and J. Llibre, Global dynamics of the Hořava-Lifshitz cosmological system, *General Relativity and Gravitation* **51**, 152, 2019.

[6] F.B. Gao and J. Llibre, Global dynamics of Hořava-Lifshitz cosmology with non-zero curvature and a wide range of potentials, *The European Physical Journal C* **80**, 137, 2020.

[7] X. Gao,Y. Wang, R. Brandenberger and A. Riotto, Cosmological perturbations in Hořava-Lifshitz gravity, *Physical Review D* **81**, 083508, 2010.

[8] G. Leon and C.R. Fadragas, Cosmological dynamical systems: and their applications, Lambert Academic Publishing, GmbH & Co. KG, Saarbrücken, 2012.

[9] G. Leon and A. Paliathanasis, Extended phase-space analysis of the Hořava-Lifshitz cosmology, *The European Physical Journal C* **79**, 746, 2019.

[10] G. Leon and E.N. Saridakis, Phase-space analysis of Hořava-Lifshitz cosmology, *Journal of Cosmology and Astroparticle Physics* **2009**, 006, 2009.

[11] E. Kiritsis and G. Kofinas, Hořava-Lifshitz cosmology, *Nuclear Physics B* **821**, 467-480, 2009.

[12] S. Lepe and J. Saavedra, On Hořava-Lifshitz cosmology, *Astrophysics and Space Science* **350**, 839-843, 2014.

[13] A. Sheykhi, S. Ghaffari and H. Moradpour, Ghost dark energy in the deformed Hořava-Lifshitz cosmology, *International Journal of Modern Physics D* **28**(06), 1950080, 2019.

[14] R. Cordero, H. García-Compeán and F.J. Turrubiates, A phase space description of the FLRW quantum cosmology in Hořava-Lifshitz type gravity, *General Relativity and Gravitation* **51**, 138, 2019.

[15] N.A. Nilsson and E. Czuchry, Hořava-Lifshitz cosmology in light of new data, *Physics of the Dark Universe* **23**, 100253, 2019.

[16] A. Paliathanasis and G. Leon, Cosmological solutions in Hořava-Lifshitz scalar field theory, *Zeitschrift für Naturforschung A* **75**(6), 523-532, 2020.

[17] E.N. Saridakis, Aspects of Hořava-Lifshitz cosmology, *International Journal of Modern Physics D* **20**(08), 1485-1504, 2011.

[18] A. Tawfik and E. Abou El Dahab, FLRW cosmology with Hořava-Lifshitz gravity: impacts of equations of state, *International Journal of Theoretical Physics* **56**(7), 2122-2139, 2017.

[19] M. Bhattacharjee, Gravitational radiation and black hole formation from gravitational collapse in theories of gravity with broken Lorentz symmetry, Baylor University, *ProQuest Dissertations Publishing* 22585106, 2019.

[20] S. Mukohyama, Hořava-Lifshitz cosmology: a review, *Classical and Quantum Gravity* **27**, 223101, 2010.

[21] T.P. Sotiriou, Hořava-Lifshitz gravity: a status report, *Journal of Physics: Conference Series* **283**, 012034, 2011.

[22] S. Carlip, Hiding the cosmological constant, *Physical Review Letters* **123**, 131302, 2019.

[23] E. Di Valentino, A. Melchiorri and J. Silk, Planck evidence for a closed universe and a possible crisis for cosmology, *Nature Astronomy* **4**, 196-203, 2020.

[24] N. Aghanim, et al. (Planck Collaboration), Planck 2018 results. V. CMB power spectra and likelihoods, *Astronomy & Astrophysics* **641**, A5, 2020.

[25] C.R. Fadragas, G. Leon and E.N. Saridakis, Dynamical analysis of anisotropic scalar-field cosmologies for a wide range of potentials, *Classical and Quantum Gravity* **31**, 075018, 2014.

[26] D. Escobar, C.R. Fadragas, G. Leon and Y. Leyva, Asymptotic behavior of a scalar field with an arbitrary potential trapped on a Randall-Sundrum's braneworld: the effect of a negative dark radiation term on a Bianchi I brane, *Astrophysics and Space Science* **349**, 575-602, 2014.

[27] A. Alho, J. Hell and C. Uggla, Global dynamics and asymptotics for monomial scalar field potentials and perfect fluids, *Classical and Quantum Gravity* **32**, 145005, 2015.

[28] F. Dumortier, J. Llibre and J.C. Artés, Qualitative theory of planar differential systems, Springer-Verlag, Berlin, 2006.

[29] M.J. Álvarez, A. Ferragut and X. Jarque, A survey on the blow up technique, *International Journal of Bifurcation and Chaos* **21**(11), 3103-3118, 2011.

[30] A. Cima and J. Llibre, Bounded polynomial vector fields, *Transactions of the American Mathematical Society* **318**(2), 557-579, 1990.

[1]School of Mathematical Science, Yangzhou University, Yangzhou 225002, China

E-mail: gaofabao@sina.com (Fabao Gao, ORCID 0000-0003-2933-1017)

[2] Departament de Matemàtiques, Universitat Autònoma de Barcelona, Bellaterra 08193, Barcelona, Catalonia, Spain

E-mail: jllibre@mat.uab.cat (Jaume Llibre, ORCID 0000-0002-9511-5999)